NK cell heparanase controls tumor invasion and immune surveillance

Eva M. Putz, … , Mark D. Hulett, Mark J. Smyth

Research Article   Immunology   Oncology

NK cells are highly efficient at preventing cancer metastasis but are infrequently found in the core of primary tumors. Here, have we demonstrated that freshly isolated mouse and human NK cells express low levels of the endo-β-D-glucuronidase heparanase that increase upon NK cell activation. Heparanase deficiency did not affect development, differentiation, or tissue localization of NK cells under steady-state conditions. However, mice lacking heparanase specifically in NK cells (*Hpse^{fl/fl} NKp46-iCre* mice) were highly tumor prone when challenged with the carcinogen methylcholanthrene (MCA). *Hpse^{fl/fl} NKp46-iCre* mice were also more susceptible to tumor growth than were their littermate controls when challenged with the established mouse lymphoma cell line RMA-S-RAE-1β, which overexpresses the NK cell group 2D (NKG2D) ligand RAE-1β, or when inoculated with metastatic melanoma, prostate carcinoma, or mammary carcinoma cell lines. NK cell invasion of primary tumors and recruitment to the site of metastasis were strictly dependent on the presence of heparanase. Cytokine and immune checkpoint blockade immunotherapy for metastases was compromised when NK cells lacked heparanase. Our data suggest that heparanase plays a critical role in NK cell invasion into tumors and thereby tumor progression and metastases. This should be considered when systemically treating cancer patients with heparanase inhibitors, since the potential adverse effect on NK cell infiltration might limit the antitumor activity of the inhibitors.

Find the latest version:

https://jci.me/92958/pdf

NK cell heparanase controls tumor invasion and immune surveillance

Eva M. Putz,[1] Alyce J. Mayfosh,[2] Kevin Kos,[1] Deborah S. Barkauskas,[1] Kyohei Nakamura,[1] Liam Town,[1] Katharine J. Goodall,[2] Dean Y. Yee,[3] Ivan K.H. Poon,[2] Nikola Baschuk,[2] Fernando Souza-Fonseca-Guimaraes,[1,4,5,6] Mark D. Hulett,[2] and Mark J. Smyth[1,4]

[1]Immunology in Cancer and Infection Laboratory, QIMR Berghofer Medical Research Institute, Herston, Queensland, Australia. [2]Department of Biochemistry and Genetics, La Trobe Institute for Molecular Science, La Trobe University, Melbourne, Victoria, Australia. [3]John Curtin School of Medical Research, The Australian National University, Canberra, Australian Capital Territory, Australia. [4]School of Medicine, The University of Queensland, Herston, Queensland, Australia. [5]Molecular Immunology Division, The Walter and Eliza Hall Institute of Medical Research, Department of Medical Biology, The University of Melbourne, Parkville, Victoria, Australia. [6]Faculty of Medicine, Dentistry and Health Sciences, University of Melbourne, Melbourne, Victoria, Australia.

NK cells are highly efficient at preventing cancer metastasis but are infrequently found in the core of primary tumors. Here, have we demonstrated that freshly isolated mouse and human NK cells express low levels of the endo-β-D-glucuronidase heparanase that increase upon NK cell activation. Heparanase deficiency did not affect development, differentiation, or tissue localization of NK cells under steady-state conditions. However, mice lacking heparanase specifically in NK cells (*Hpse^fl/fl NKp46-iCre* mice) were highly tumor prone when challenged with the carcinogen methylcholanthrene (MCA). *Hpse^fl/fl NKp46-iCre* mice were also more susceptible to tumor growth than were their littermate controls when challenged with the established mouse lymphoma cell line RMA-S-RAE-1β, which overexpresses the NK cell group 2D (NKG2D) ligand RAE-1β, or when inoculated with metastatic melanoma, prostate carcinoma, or mammary carcinoma cell lines. NK cell invasion of primary tumors and recruitment to the site of metastasis were strictly dependent on the presence of heparanase. Cytokine and immune checkpoint blockade immunotherapy for metastases was compromised when NK cells lacked heparanase. Our data suggest that heparanase plays a critical role in NK cell invasion into tumors and thereby tumor progression and metastases. This should be considered when systemically treating cancer patients with heparanase inhibitors, since the potential adverse effect on NK cell infiltration might limit the antitumor activity of the inhibitors.

Introduction

Extracellular matrix (ECM) comprises more than 50 different proteins, with the main components being large insoluble proteins such as type IV collagen, laminin, and heparan sulphate proteoglycans (HSPGs), creating a barrier that is difficult for immune cells to cross. Many solid tumors are encapsulated by a dense layer of the ECM that makes it particularly difficult for immune cells to infiltrate. Several studies have shown that NK and other immune cells tend to accumulate in the stroma of the invasive margin rather than invade the tumor core itself (1, 2), ultimately limiting effective antitumor immunity (3).

HSPGs constitute a major part of the ECM (4). In mammals, the only enzyme known to degrade HSPGs is the endo-β-D-glucuronidase heparanase. There is only 1 enzymatically active form of heparanase in mammals that is expressed at very low levels in normal tissues, and heparanase deficiency in mice causes no obvious pathophysiologies (5, 6). Heparanase is secreted as an enzymatically inactive pro-heparanase and requires reuptake into the cell and processing by cathepsin-L in lysosomes (7) or α granules (8) in order to give rise to the enzymatically active heparanase protein. In

recent years, it has become evident that heparanase is a complex protein with both enzymatic and nonenzymatic activities, depending on its location and cleavage (9–13). The degradation of HSPGs and remodeling of the ECM require the enzymatically active heparanase protein to be secreted into the extracellular space. HSPGs bind a range of proteins including angiogenic factors, growth factors, and cytokines that are released into the ECM upon degradation by heparanase and induce tissue remodeling, angiogenesis, and chronic inflammation. Tumor cell–derived heparanase contributes to all these processes, thereby sustaining tumor cell proliferation, vascularization, and metastasis. It is therefore not surprising that the expression of heparanase is frequently upregulated in malignant cells and correlates with poor prognosis and metastatic potential (14–16). Heparanase is thus considered a highly promising target for anticancer therapy, and the first clinical trials using heparan sulfate (HS) mimetics have enrolled patients.

Besides tumor cells, a number of normal cell types, such as endothelial and immune cells including NK cells, express heparanase (17). Recently generated heparanase gene–targeted (*Hpse*-targeted) mice were used to investigate the role of heparanase in immune cell subtypes in response to different stimuli. Whereas heparanase was proven important for the migration of DCs (6, 18) and eosinophils (19) in response to inflammation and allergic sensitization, heparanase appeared dispensable for the extravasation of mouse neutrophils and T cells under inflammatory conditions (19, 20). In contrast, heparanase reportedly enhances the tumor
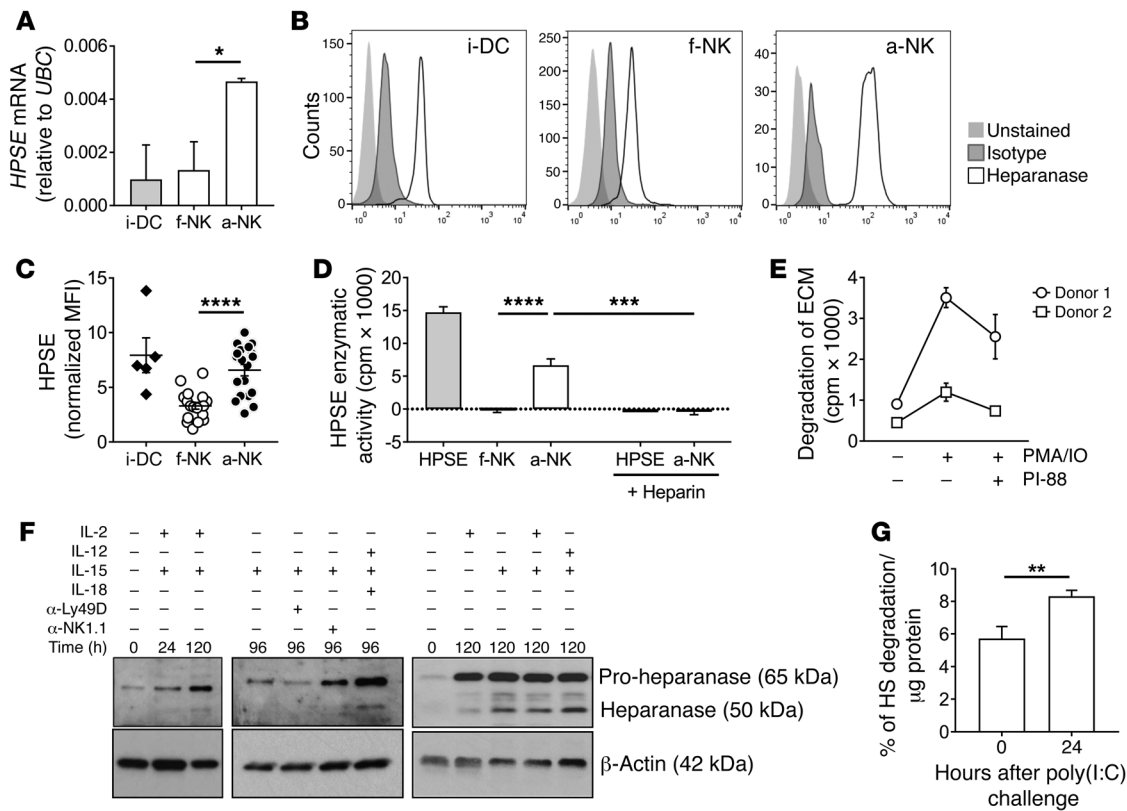
Figure 1. Activated NK cells express enzymatically active heparanase. (**A**–**E**) NK cells isolated from human donors were assayed as f-NK or a-NK cells. i-DCs were included as a control. (**A**) mRNA expression of *HPSE* relative to *UBC* was assessed by quantitative PCR (qPCR) (mean ± SD; *n* = 3 individual donors; 1 representative experiment of 2 experiments). (**B** and **C**) Heparanase protein expression was determined by intracellular staining and flow cytometry (mean ± SEM; *n* = 5–13 donors per group). MFI, mean fluorescence intensity. (**D**) HPSE enzymatic activity was determined by incubating 2×10^5 f-NK or a-NK cells with ³H-HS for 16 hours ± 1 U heparin. Human platelet heparanase (2.5 ng) was included as a control (mean ± SEM; *n* = 4–11 per group; data were pooled from 2 independent experiments). (**E**) a-NK cells (2×10^6) from 2 individual donors were cultured on ³⁵S-ECM plates ± 2 ng/ml PMA/0.1 μM ionomycin (IO) ± 200 μg/ml PI-88. ECM degradation was measured after 20 hours (mean ± SD; *n* = 3 technical replicates; data are representative of 5 individual donors). (**F**) Heparanase expression was analyzed by Western blotting. FACS-purified mouse TCRβ⁻NK1.1⁺NKp46⁺DX5⁺ NK cells were analyzed ex vivo or after stimulation for the indicated durations by cytokines (500 U/ml IL-2, 1 ng/ml IL-12, 10 ng/ml IL-15, and 10 ng/ml IL-18) or by NK cell receptor cross-linking (α-Ly49D or α-NK1.1). (**G**) The enzymatic activity of heparanase was determined by a TR-FRET–based HS degradation assay. Splenic NK cells were isolated by negative depletion from WT mice that had been injected with 250 μg poly(I:C) 24 hours prior to the analysis or were left untreated (mean ± SD; *n* = 3). Statistically significant differences between the groups were determined by 1-way ANOVA with Tukey's post test (**A**, **C**, and **D**) or unpaired Student's *t* test (**G**). **P* < 0.05, ***P* < 0.01, ****P* < 0.001, and *****P* < 0.0001.

infiltration and effectiveness of adoptively transferred cytotoxic T cells (21). Interestingly, while short-term activation of T cells induced the expression of heparanase, long-term in vitro expansion of human T cells downregulated heparanase expression, which was responsible for the impaired invasion of stroma-rich tumors in vivo and Matrigel in vitro (21). These studies highlight the importance of heparanase, but also the differences between immune cell types and model systems.

Here, we investigated the expression and function of heparanase in human and mouse NK cells. Whereas freshly isolated NK cells express very low levels of heparanase, the expression is upregulated upon cytokine stimulation or NK cell receptor cross-linking. By generating conditional heparanase gene–targeted (floxed) mice specifically lacking the *Hpse* gene in NKp46⁺ cells (*Hpse*^fl/fl^ *NKp46-iCre* mice), we showed that heparanase expression in NK cells was indispensable for efficient invasion and subsequent tumor surveillance. The initiation of methylcholanthrene-induced fibrosarcoma, the growth of primary RMA-S-RAE-1β tumors, and the lung

metastases of tumor cell lines (B16F10, LWT1, RM-1, and E0771) were exacerbated in *Hpse*^fl/fl^ *NKp46-iCre* mice. Thus, this study is the first to our knowledge to define heparanase expression and activity of major importance in the tumor-invasive potential and antitumor activity of NK cells.

Results

Activated NK cells express enzymatically active heparanase. Whereas heparanase is highly abundant in platelets and tumor cells, its expression is rather limited in the majority of other tissues and immune cell types (8). Human NK cells freshly isolated from peripheral blood mononuclear cells (PBMCs) (f-NK cells) expressed low levels of HPSE mRNA (Figure 1A) and protein (Figure 1, B and C), comparable to what has been observed with immature human DCs (i-DCs) (22). Activation of NK cells with B-LCL and IL-2 in culture for 18 days (a-NK cells) significantly induced the transcription of the *HPSE* gene (Figure 1A) and enhanced heparanase protein levels by approximately 2-fold (Figure 1, B and C). Notably, the hepara-
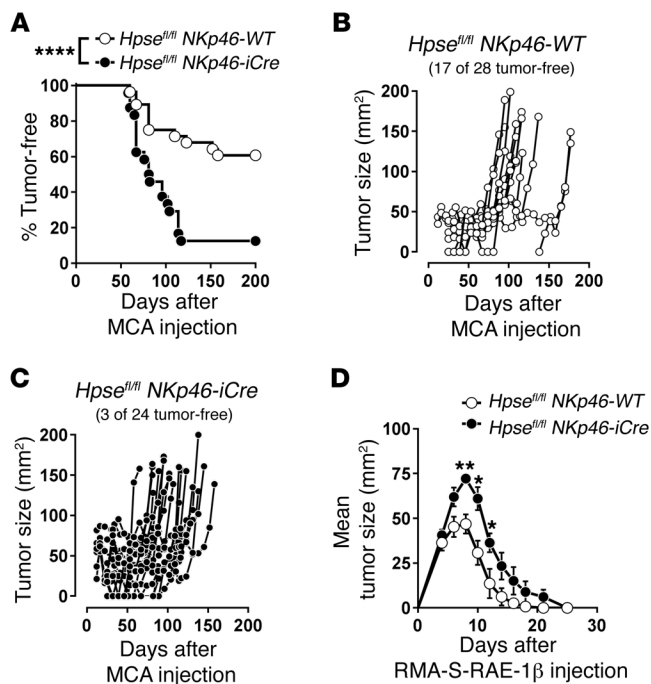
Figure 2. NK cell–intrinsic heparanase is indispensable for efficient surveillance of MCA-induced fibrosarcoma and RAE-1–expressing lymphoma. (A–C) *Hpse^fl/fl NKp46-WT* and *Hpse^fl/fl NKp46-iCre* mice were inoculated s.c. in the hind flank with 100 μg MCA in 0.1 ml corn oil. Mice were then monitored over a 200-day period for fibrosarcoma development. Tumors were measured every week with a caliper (*n* = 24–28 per group; data were pooled from 2 independent experiments). **(A)** Data were recorded as the percentage of tumor-free mice (tumors were defined as measuring >3 mm in diameter and consistently growing). Tumor growth curves of individual **(B)** *Hpse^fl/fl NKp46-WT* and **(C)** *Hpse^fl/fl NKp46-iCre* mice. **(D)** *Hpse^fl/fl NKp46-WT* and *Hpse^fl/fl NKp46-iCre* mice were injected s.c. with 5 × 10^6 RMA-S-RAE-1β cells. Tumor growth was measured every 2 to 3 days with a caliper (mean ± SEM; *n* = 7 per group; 1 representative experiment of 2 experiments). Statistically significant differences were determined by log-rank Mantel-Cox test **(A)** and Mann-Whitney *U* test **(D)**. *$P < 0.05$, **$P < 0.01$, and ****$P < 0.0001$.

nase present in f-NK cells did not possess any measurable enzymatic activity. However, upon activation, NK cells clearly exhibited enzymatic activity (Figure 1D) and an improved ability to degrade artificial ECM (Figure 1E), which was abrogated by the natural heparanase antagonist heparin (Figure 1D) and the pharmaceutical heparanase inhibitor PI-88 (Figure 1E), respectively.

Likewise, mouse NK cells freshly isolated from splenocytes expressed low levels of heparanase (Figure 1F, lanes 1 and 8), whereas heparanase was strongly induced upon NK cell activation, irrespective of the nature of the in vitro stimulation (Figure 1F). The upregulation of heparanase was a rather slow process that showed the highest expression levels 4–5 days after stimulation by cytokines (IL-2, IL-12, IL-15, and IL-18) or NK cell receptor cross-linking (anti-NK1.1) (Figure 1F). To understand whether the heparanase produced by NK cells in vivo was enzymatically active, mice were challenged with immune-activating poly(I:C). Compared with NK cells from naive mice, we found that activated NK cells showed an enhanced capacity to degrade HS (Figure 1G).

In order to investigate the molecular function of heparanase, we generated gene-modified mouse strains: (1) carrying a complete knockout of heparanase in the entire mouse (*Hpse^-/-*, Supplemental Figure 1A; supplemental material available online with this article; https://doi.org/10.1172/JCI92958DS1); and (2) carrying the conditional deletion of heparanase in NKp46+ cells, which was achieved by crossing mice harboring loxP-flanked heparanase alleles with *NKp46-iCre* knock-in mice, in which the improved Cre-recombinase (i-Cre) was inserted into the NKp46 locus (*Hpse^fl/fl NKp46-iCre* versus *Hpse^fl/fl NKp46-WT*, Supplemental Figure 1B). In line with the low expression of heparanase in naive conventional NKp46+ NK cells (c-NKs), heparanase deficiency did not affect NK cell proportions, absolute NK cell counts, or the expression of maturation or other NK cell–surface markers (i.e., CD27, CD11b, KLRG1, NKG2A/C/E, NKG2D, CD122, and CD226) in peripheral blood or various organs in which NK cells

typically recirculate (Supplemental Figure 2). Additionally, the number and phenotype of liver-resident NKp46-expressing type 1 innate lymphoid cells (ILC1) cells were unaltered by heparanase deficiency (Supplemental Figure 3, A–D). It is noteworthy that we failed to detect heparanase protein in ILC1 or c-NKs freshly isolated from the livers of WT mice (Supplemental Figure 3E).

In summary, naive mouse and human NK cells express only low levels of enzymatically active heparanase, but upon activation, heparanase expression is increased. Heparanase deficiency does not appear critical for normal tissue residency and recirculation of NKp46+ immune cells, nor for the development and differentiation of the NK cell lineage.

NK cell–intrinsic heparanase is indispensable for efficient tumor surveillance. Although heparanase is dispensable for NK cell localization within healthy tissues, NK cells may require heparanase to migrate through tumor stroma. Therefore, we challenged *Hpse^fl/fl NKp46-iCre* and *Hpse^fl/fl NKp46-WT* mice in the de novo fibrosarcoma model, in which mice were administered a s.c. injection of 100 μg methylcholanthrene (MCA). Host resistance to tumor initiation was previously shown to be highly dependent on NK cells (23). Fibrosarcomas arose in 39% of the control *Hpse^fl/fl NKp46-WT* mice over the course of 200 days. In contrast, within the same observation period, 88% of *Hpse^fl/fl NKp46-iCre* mice developed fibrosarcomas (Figure 2A). Although the prevalence was significantly higher in *Hpse^fl/fl NKp46-iCre* mice, the growth kinetics of the individual tumors was similar in *Hpse^fl/fl NKp46-iCre* and *Hpse^fl/fl NKp46-WT* mice once the tumors were established (Figure 2, B and C). This is consistent with the early role of NK cells in preventing tumor initiation but not tumor growth.

NK cells can be strongly activated in vivo by tumors overexpressing ligands that activate NK cell receptors (24, 25). To test the role of NK cell heparanase in such a setting, we injected *Hpse^fl/fl NKp46-iCre* and *Hpse^fl/fl NKp46-WT* control mice s.c. with the lymphoma cell line RMA-S-RAE-1β. This cell line is deficient in
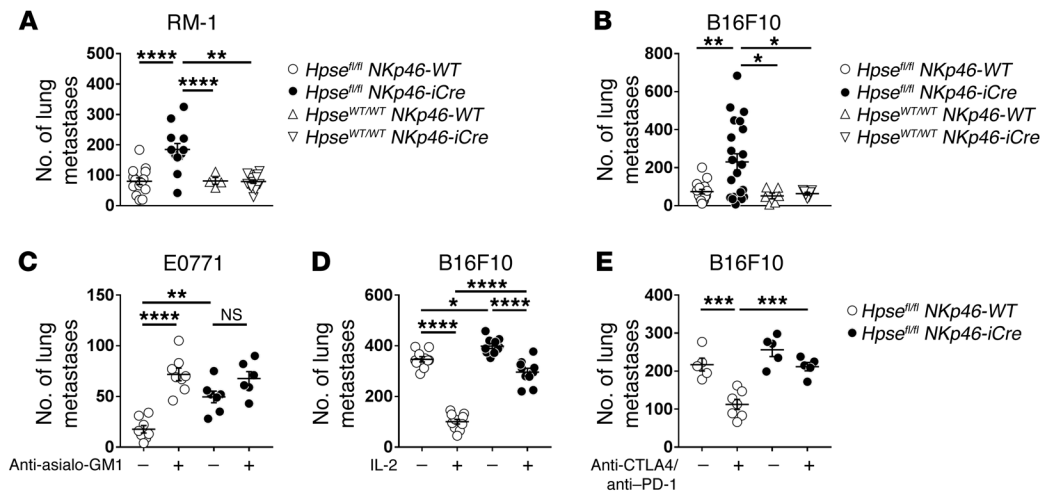
Figure 3. Heparanase-deficient NK cells display impaired control of lung metastases. (**A**) $Hpse^{fl/fl}$ $NKp46$-WT, $Hpse^{fl/fl}$ $NKp46$-$iCre$, $Hpse^{WT/WT}$ $NKp46$-WT (B6.WT), and $Hpse^{WT/WT}$ $NKp46$-$iCre$ mice were injected i.v. with 1×10^5 RM-1 prostate carcinoma cells. Lungs were harvested on day 14 and macrometastases counted (mean ± SEM; n = 4–16 mice per group; data were pooled from 2 independent experiments). (**B**) $Hpse^{fl/fl}$ $NKp46$-WT, $Hpse^{fl/fl}$ $NKp46$-$iCre$, $Hpse^{WT/WT}$ $NKp46$-WT (B6.WT), and $Hpse^{WT/WT}$ $NKp46$-$iCre$ mice were injected i.v. with 2×10^5 B16F10 melanoma cells. Lungs were harvested on day 14 and macrometastases counted (mean ± SEM; n = 6–22 mice per group; data were pooled from 3 independent experiments). (**C**) $Hpse^{fl/fl}$ $NKp46$-WT and $Hpse^{fl/fl}$ $NKp46$-$iCre$ mice were injected with 2×10^4 E0771 cells into the mammary fat pad and treated with either 50 μg control Ig (–) or anti–asialo-GM1 (+) (NK cell depletion) on days –1, 0, 7, 14, and 23 after tumor transplantation. Tumors were removed surgically on day 12. Lungs were harvested on day 35 and macrometastases counted (mean ± SEM; n = 6–8 mice per group). (**D**) $Hpse^{fl/fl}$ $NKp46$-WT and $Hpse^{fl/fl}$ $NKp46$-$iCre$ mice were injected i.v. with 5×10^5 B16F10 melanoma cells and treated i.p. with either PBS or 100,000 IU IL-2 on days 0, 1, 2, 3, and 4. Lungs were harvested on day 14 and macrometastases counted (mean ± SEM; n = 10–11 mice per group; data were pooled from 2 independent experiments). (**E**) $Hpse^{fl/fl}$ $NKp46$-WT and $Hpse^{fl/fl}$ $NKp46$-$iCre$ mice were injected i.v. with 5×10^5 B16F10 melanoma cells and treated with either 500 μg control Ig (–) or 250 μg each of anti-CTLA4 and anti-PD-1 (+) on days 0 and 3 after injection, respectively. Lungs were harvested on day 14 and macrometastases counted (mean ± SEM; n = 5–7 mice per group). (**A**–**E**) Statistically significant differences between the groups were determined by 1-way ANOVA with Tukey's post test (*P < 0.05, **P < 0.01, ***P < 0.001, and ****P < 0.0001).

MHC class I expression, but overexpresses the NK cell group 2D (NKG2D) ligand RAE-1β and thus represents a highly immunogenic tumor that is typically rejected in an NK cell–dependent manner. RMA-S-RAE-1β tumors grew significantly larger in $Hpse^{fl/fl}$ $NKp46$-$iCre$ mice when compared with tumor growth in $Hpse^{fl/fl}$ $NKp46$-WT control mice, indicative of an ineffective or delayed NK cell response (Figure 2D). Although the tumor suppression was slightly delayed in $Hpse^{fl/fl}$ $NKp46$-$iCre$ mice, all inoculated mice eventually rejected their tumors (Figure 2D), consistent with the very strong effect of RAE-1 ligands.

NK cell heparanase is critical for the effective suppression of tumor metastases. Host control of experimental metastases acts in both the periphery upon tumor seeding and within the lung niche tissue, where the tumor colonies develop. Interestingly, $Hpse^{fl/fl}$ $NKp46$-$iCre$ mice were significantly more susceptible to experimental tumor metastasis than were control mice when challenged with the prostate carcinoma cell line RM-1 (Figure 3A) or the melanoma cell lines LWT1 (Supplemental Figure 4A) or B16F10 (Figure 3B). Similar experiments using the global deletion of heparanase ($Hpse^{-/-}$) revealed a minor increase in the experimental metastasis of RM-1 and B16F10 compared with that seen in WT controls, but $Hpse^{fl/fl}$ $NKp46$-$iCre$ mice were significantly more susceptible to metastasis (Supplemental Figure 5). All of these experimental metastatic tumors were previously reported to be critically controlled by host NK cells (26, 27) (Supplemental Figure 4B). Further, the occurrence of spontaneous metastasis of orthotopically transplanted E0771 mammary carcinoma cells into the lungs was significantly higher in $Hpse^{fl/fl}$ $NKp46$-$iCre$ mice than in $Hpse^{fl/fl}$

$NKp46$-WT mice (Figure 3C). In line with previous reports (26, 27), NK cell depletion in $Hpse^{fl/fl}$ $NKp46$-WT mice significantly enhanced the spontaneous formation of metastases (Figure 3C). In contrast, NK cell depletion in $Hpse^{fl/fl}$ $NKp46$-$iCre$ mice did not significantly increase the spontaneous metastasis of E0771, suggesting that the antimetastatic properties of heparanase-deficient NK cells were negligible in this model. Given the impact of heparanase on innate NK cell antimetastatic activity, we next tested its importance in immunotherapy. Here, we inoculated B16F10 melanoma cell–bearing $Hpse^{fl/fl}$ $NKp46$-$iCre$ and $Hpse^{fl/fl}$ $NKp46$-WT mice with high doses of recombinant IL-2. While this treatment significantly decreased the number of lung metastases in both $Hpse^{fl/fl}$ $NKp46$-$iCre$ and $Hpse^{fl/fl}$ $NKp46$-WT mice, the antimetastatic effect of IL-2 was significantly stronger in $Hpse^{fl/fl}$ $NKp46$-WT mice (Figure 3D). Similarly, the contemporary therapy for advanced human melanoma, which involves the combination of anti-CTLA4 and anti–PD-1 treatment, efficiently reduced B16F10 lung metastases in $Hpse^{fl/fl}$ $NKp46$-WT mice. In contrast, this therapy largely failed in $Hpse^{fl/fl}$ $NKp46$-$iCre$ mice (Figure 3E).

Collectively, our data indicated that NK cell–intrinsic expression of heparanase plays a crucial role in the ability of NK cells to confer antitumor immunity in mouse models of carcinogen-induced tumor initiation, primary tumor growth, and tumor metastasis.

NK cell proliferation and function are unchanged by loss of heparanase. The increased tumor susceptibility of $Hpse^{fl/fl}$ $NKp46$-$iCre$ mice (Figures 2 and 3) might potentially be linked to defects in NK cell survival, proliferation, or function in the absence of heparanase. To test these hypotheses, we isolated NK cells from $Hpse^{fl/fl}$ $NKp46$-
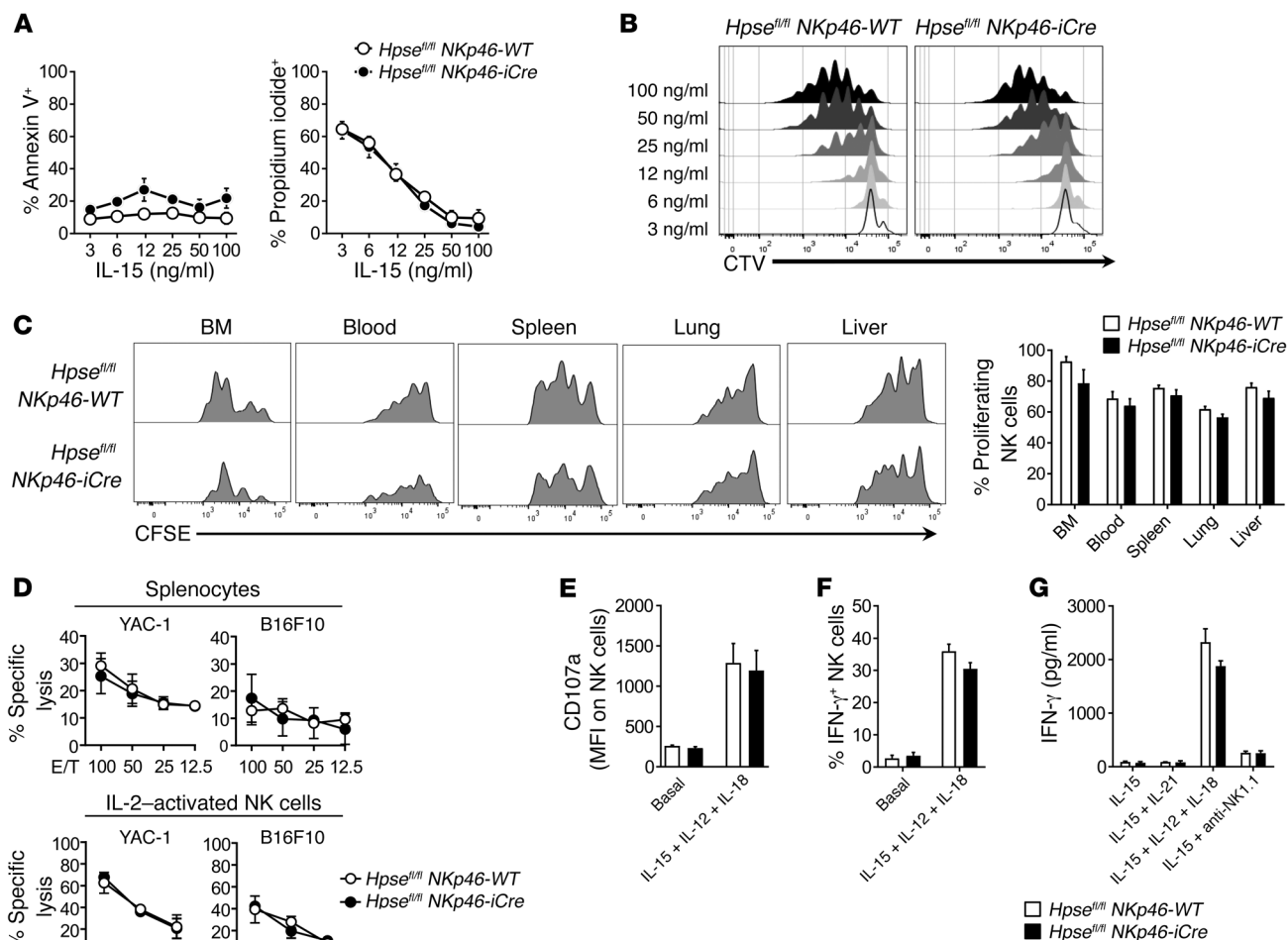
Figure 4. NK cell proliferation and function are unchanged by loss of heparanase. (**A** and **B**) Purified BM NK cells from *Hpse^fl/fl^ NKp46-WT* or *Hpse^fl/fl^ NKp46-iCre* mice were labeled with CTV and cultured for 3 days in IL-15 as indicated (mean ± SD; *n* = 2 biological replicates). (**A**) Apoptosis was determined by annexin V and propidium iodide staining. (**B**) Proliferation was assessed by CTV dilution. (**C**) Purified splenic CFSE-labeled NK cells (2 × 10^5^) were injected i.v. into B6.*Rag2^–/–^ Il2rg^–/–^* mice. After 3 days, the proliferation of CD45^+^TCRβ^−^NK1.1^+^DX5^+^ NK cells in the indicated organs was determined by flow cytometry. Flow cytometric plot shows a representative proliferation profile. Data in the bar graph were pooled from 2 independent experiments (mean ± SEM; *n* = 8 per group). (**D**) The cytotoxicity of freshly isolated splenocytes or IL-2–activated NK cells (1,000 U/ml for 5 days) against YAC-1 and B16F10 target cells was tested at the indicated E/T ratios after 4 hours (mean ± SD; *n* = 3 biological replicates; 1 representative experiment of 2 experiments). (**E**) Splenocytes (5 × 10^6^) were stimulated for 4 hours with 1 ng/ml IL-12, 100 ng/ml IL-15, and 10 ng/ml IL-18, and the expression of CD107a was assessed on TCRβ^−^NK1.1^+^DX5^+^ NK cells (mean ± SD; *n* = 4 mice per group). (**F**) Lung cells were stimulated for 4 hours in 1 ng/ml IL-12, 100 ng/ml IL-15, and 10 ng/ml IL-18, and the production of IFN-γ was measured by intracellular staining (mean ± SEM; *n* = 10; data were pooled from 3 independent experiments). (**G**) Purified splenic NK cells were stimulated in 50 ng/ml IL-15, 100 ng/ml IL-21, 1 ng/ml IL-12, 10 ng/ml IL-18, or anti-NK1.1 precoated wells. The release of IFN-γ was measured after 24 hours by CBA (mean ± SD; *n* = 2 biological replicates; 1 representative experiment of 2 experiments).

iCre and *Hpse^fl/fl^ NKp46-WT* mice and cultivated them in vitro for 3 days in the presence of different concentrations of recombinant IL-15. We did not detect any differences in NK cell survival as assessed by annexin V and propidium iodide staining (Figure 4A). The in vitro proliferation of *Hpse^fl/fl^ NKp46-iCre* and *Hpse^fl/fl^ NKp46-WT* NK cells was similar as measured by CellTrace Violet (CTV) dilution (Figure 4B). In concert with these findings, we did not observe any differences in the in vivo proliferation of CFSE-labeled *Hpse^fl/fl^ NKp46-iCre* or *Hpse^fl/fl^ NKp46-WT* NK cells after transplantation into immunodeficient *Rag2^–/–^ Il2rg^–/–^* mice (Figure 4C).

Since the impaired antitumor function of heparanase-deficient NK cells was not related to alterations in NK cell proliferation or survival, we next asked whether a lack of heparanase impacted

NK cell effector functions. In vitro cytotoxicity assays performed with either freshly isolated splenocytes or IL-2–stimulated splenic NK cells from *Hpse^fl/fl^ NKp46-iCre* and *Hpse^fl/fl^ NKp46-WT* mice against YAC-1 and B16F10 target cells in various effector-to-target (E/T) ratios showed no differences between the strains (Figure 4D). Accordingly, *Hpse^fl/fl^ NKp46-iCre* and *Hpse^fl/fl^ NKp46-WT* NK cells possessed the same capacity to degranulate after stimulation in vitro, as measured by CD107a staining (Figure 4E). Besides direct killing of tumor cells, NK cells produce significant amounts of cytotoxic and immunomodulatory cytokines that are crucial for antitumor responses. However, loss of heparanase did not affect the production (Figure 4F) or release of IFN-γ (Figure 4G), TNF (Supplemental Figure 4C), or the chemokines CCL3, CCL4, and
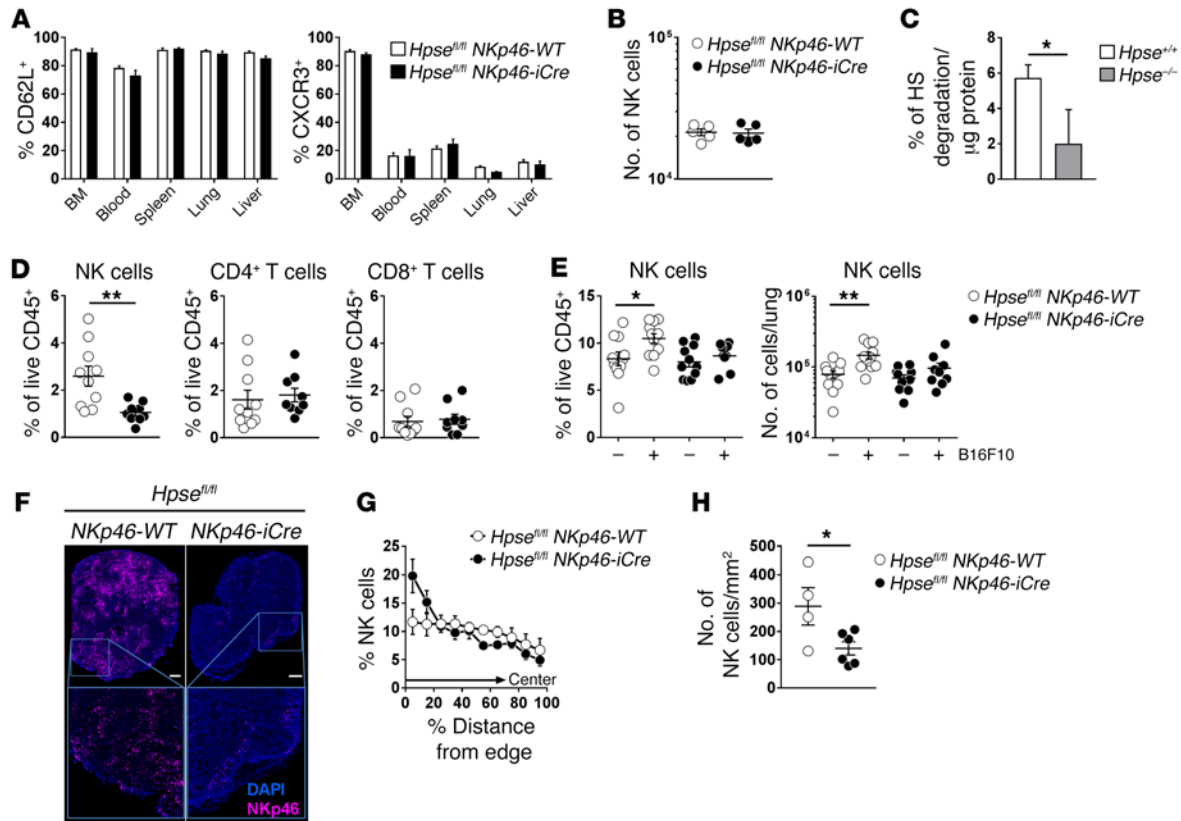
Figure 5. NK cell invasion is impaired in the absence of heparanase. (**A**) The expression of CD62L and CXCR3 on TCRβ⁻NK1.1⁺DX5⁺ NK cells was analyzed by flow cytometry in the indicated organs of *Hpse^fl/fl^ NKp46-WT* and *Hpse^fl/fl^ NKp46-iCre* mice (mean ± SEM; *n* = 3–10). (**B**) Preactivated splenic NK cells (7.5 × 10⁴) were seeded in the upper chamber of a Transwell insert. The number of migrating cells in response to 10% FBS and 20 ng/ml CXCL10 was assessed after 17 hours (mean ± SEM; *n* = 5; data were pooled from 2 independent experiments). (**C**) Heparanase enzymatic activity of isolated *Hpse^+/+^* and *Hpse^−/−^* splenic NK cells was determined by a TR-FRET–based HS degradation assay (mean ± SD; *n* = 3). (**D**) Mice were injected s.c. with 100 μl Matrigel. Leukocyte infiltration into the Matrigel plugs was determined by flow cytometry after 3 days. Depicted are TCRβ⁻NK1.1⁺NKp46⁺ NK, TCRβ⁺CD4⁺, and TCRβ⁺CD8⁺ T cells, respectively (mean ± SEM; *n* = 9–10 mice per group; data were pooled from 3 independent experiments). (**E**) Mice were injected i.v. with 5 × 10⁵ B16F10 melanoma cells. Lungs were harvested after 24 hours, and NK cell proportions and numbers were determined by flow cytometry (mean ± SEM; *n* = 9–12 mice per group; data were pooled from 3 independent experiments; direct comparison of NK cell proportions between B16F10 challenged *NKp46-WT* and *NKp46-iCre* mice *P* = 0.0118, Mann-Whitney *U* test, and NK cell numbers between B16F10 challenged *NKp46-WT* and *NKp46-iCre* mice: *P* = 0.0278, Mann-Whitney *U* test). (**F**–**H**) Mice were injected s.c. with 5 × 10⁶ RMA-S-RAE-1β cells. Tumors were harvested on day 5 and analyzed by immunofluorescence (mean ± SEM; *n* = 4–6 per group). (**F**) Representative images of sections stained for NKp46⁺ NK cells (magenta) and DAPI (blue). Scale bars: 500 μm. Original magnification: ×20, tiled scan of whole tumor. (**G**) The distance of individual NK cells from the edge was calculated. (**H**) The number of NKp46⁺ cells per section was quantified by Imaris. Statistically significant differences were determined by Student's *t* test (**C**), Mann-Whitney *U* test (**D** and **H**), or 1-way ANOVA with Tukey's post test (**E**). **P* < 0.05 and ***P* < 0.01.

CCL5 (data not shown) by cytokine-activated or receptor–cross-linked NK cells. Similarly, when challenged in vivo with LPS, *Hpse^fl/fl^ NKp46-iCre* and *Hpse^fl/fl^ NKp46-WT* NK cells produced comparable levels of IFN-γ and TNF (Supplemental Figure 4, D and E).

In summary, the increased tumor susceptibility of heparanase-deficient mice could not be explained by differences in NK cell survival, proliferation, cytotoxicity, or cytokine production.

NK cell invasion is significantly impaired in the absence of heparanase. Considering the ample evidence of the involvement of heparanase in the transmigration of cells through the ECM and the basal membrane (28), we next examined whether heparanase deficiency affected NK cell migration and invasion. Loss of heparanase did not affect the surface expression of the migration marker CD62L or the chemokine receptors CXCR3, CXCR4, or CCR2 on NK cells when analyzed ex vivo in different organs or after stimulation in vitro (Figure 5A and Supplemental Figure 6). Importantly,

the expression of heparanase was clearly dispensable for the simple chemokine-induced migration of NK cells as determined in a Transwell assay (Figure 5B). In contrast, heparanase deficiency significantly impaired the ability of NK cells to degrade HS chains in vitro (Figure 5C) and to invade the artificial ECM in vivo (Figure 5D). Matrigel plugs introduced s.c. contained fewer invading NK cells in *Hpse^fl/fl^ NKp46-iCre* mice than in *Hpse^fl/fl^ NKp46-WT* mice, whereas other immune cell types, including CD4⁺ and CD8⁺ T cells, infiltrated the plugs to the same degree (Figure 5D).

Considering the increased tumor susceptibility of *Hpse^fl/fl^ NKp46-iCre* mice, we next assessed whether heparanase impacted the migration of NK cells into the tumor-bearing organs. We found that fewer *Hpse^fl/fl^ NKp46-iCre* NK cells infiltrated s.c. injected RMA-S-RAE-1β tumors (Figure 5, F–H), while CD4⁺ and CD8⁺ T cell frequencies were unchanged (Supplemental Figure 7A). The tumors were harvested 5 days after injection, and at this early

time point, the tumor weights were similar in both *Hpse^fl/fl NKp46-iCre* and *Hpse^fl/fl NKp46-WT* mice (Supplemental Figure 7B). As assessed by immunofluorescence staining, heparanase-deficient NK cells showed an impaired invasive capacity, which was quantified by the distance traveled into the tumor (Figure 5G). Ultimately, significantly fewer *Hpse^fl/fl NKp46-iCre* NK cells were found in the tumor (Figure 5H), a finding that could not be related to any alterations in the proliferation of intratumoral NK cells (Supplemental Figure 7C). NK cells infiltrated the lungs of *Hpse^fl/fl NKp46-WT* mice within 24 hours after i.v. injection of B16F10 cells. In contrast, we did not observe this increase in NK cell numbers in the tumor-bearing lungs of *Hpse^fl/fl NKp46-iCre* mice (Figure 5E). We found that T cell numbers and proportions were unchanged (Supplemental Figure 7D).

In summary, these data showed that heparanase plays an important role in NK cell invasion of Matrigel and tumors, probably by facilitating the breakdown of HS chains and the subsequent degradation of the ECM. The heparanase-mediated effect on NK cell invasion was independent of the expression of migration markers or chemokine receptors by NK cells.

Discussion
Despite the potency of NK cells against metastases and hematological cancers (29), their utility against solid tumors and our knowledge about their requirements for tumor infiltration are limited (1, 2, 30–32). Here, we report that NK cells express significant levels of heparanase that are strongly induced upon cell activation. Heparanase produced by NK cells exhibits enzymatic activity and is able to degrade ECM, which is reportedly a prerequisite for cell invasion and migration across a basement membrane (28). By using gene-modified mice with heparanase specifically deleted in NK cells, we showed that NK cell–intrinsic heparanase was indispensable for efficient tumor immunosurveillance. *Hpse^fl/fl NKp46-iCre* mice were highly prone to de novo MCA-induced fibrosarcoma, transplanted lymphoma overexpressing NKG2D ligand, and experimental lung metastases of B16F10 melanoma, LWT1 melanoma, and RM-1 prostate carcinoma. *Hpse^fl/fl NKp46-iCre* mice were also more susceptible to the spontaneous metastasis of E0771 mammary carcinoma. The increased tumor susceptibility correlated with significant impairments in NK cell, but not T cell, infiltration of Matrigel and tumor-bearing organs in the absence of NK cell heparanase. Furthermore, immunotherapies, such as high-dose IL-2 and immune checkpoint anti–PD-1/anti-CTLA4 mAbs in combination, were suboptimal in the absence of NK cell heparanase. Our data suggest that heparanase plays a critical role in NK cell invasion and tumor immunosurveillance and highlight the importance of inducing and maintaining heparanase activity to optimize NK cell functions against tumors.

The presence of tumor-infiltrating NK cells is associated with good prognosis (33–35), however, whether the primary function of tumor-infiltrating NK cells is to directly kill the malignant cells or to produce cytokines that will modulate the tumor, the stroma, or other immune cells in the microenvironment is still a matter of investigation. In the Matrigel and tumor model assays we examined, loss of heparanase in NK cells decreased NK cell localization in tumors, but was without an indirect effect on T cell subsets. In the MCA-induced fibrosarcoma model, NK cell–derived IFN-γ is a critical fac-

tor responsible for the formation of a fibrotic reaction enclosing the carcinogen and preventing tumor outgrowth (e.g., the foreign body reaction) (36). We hypothesize that the higher incidence of fibrosarcoma observed in the absence of NK cell heparanase is a result of fewer tumor-infiltrating NK cells, a reduced fibrotic reaction, and, consequently, a more frequent tumor initiation and outgrowth. Interestingly, some tumor tissues were shown to contain high levels of chemokines, which promoted the infiltration of T cells, but failed to do so for NK cells (1). It thus seems that, although the recruitment signals might be provided by the tumor microenvironment, NK cells are unable to infiltrate a solid tumor in sufficient numbers. NK cell accumulation in tumors was previously shown to be regulated by IFN-γ and CXCL10 (37). Our data demonstrated that the expression of CXCR3 — the receptor for CXCL10 — and other adhesion molecules, such as L-selectin (also known as CD62L), was unaffected by the absence of NK cell heparanase. Therefore, we believe that the diminished invasive potential of heparanase-deficient NK cells is not attributable to defects in chemokine signaling but rather a result of impaired degradation of the ECM.

Even though we have shown that a function of heparanase in NK cells is to break down the ECM, the role of heparanase extends beyond tissue invasion in other immune cell subsets. For example, pro-heparanase can induce cell signaling via PI3-kinase–mediated phosphorylation of AKT (38, 39) and even act as a transcription factor regulating genes involved in cell differentiation, inflammation, and glucose metabolism (40–42). Other studies reported that heparanase enzymatic activity upregulates proinflammatory cytokines from human peripheral blood leukocytes (IL-1β, IL-6, IL-8, IL-10, and TNF), as well as mouse splenocytes (IL-6, MCP-1, and TNF) (43). Furthermore, heparanase silencing by siRNA has been shown to reduce the capacity of Jurkat T cells to produce cytokines such as IFN-γ and IL-2 (41). Recently, Gutter-Kapon et al. reported a 2-fold slower growth of Lewis lung carcinoma (LLC) implanted s.c. into heparanase-deficient mice when compared with WT mice (44). They showed that heparanase-deficient macrophages had reduced motility, reduced infiltration into LLC tumors, and an altered phagocytic capacity that was partly independent of heparanase enzymatic activity. These data are interesting in light of the different levels of metastasis we observed between *Hpse^+/+* (WT), *Hpse^−/−*, and *NKp46-iCre* strains, since it is possible that deleting *Hpse* in NK cells promotes metastasis, while deleting *Hpse* in some myeloid cell populations may reduce metastasis. Consequently, the (global) *Hpse^−/−* phenotype appears more similar to that of WT controls than does the conditional deficiency of *Hpse* in NK cells (*NKp46-iCre*). Another study found that the antitumor effect of the HS mimetic PG545, an inhibitor of heparanase, in mice was dependent on DC-mediated IL-12 production that led to NK cell activation and accumulation in the tumor (45). In comparison, our findings show that NK cell–intrinsic loss of heparanase did not affect NK cell development, survival, cytotoxic function, or cytokine production, but significantly impaired tumor immunosurveillance leading to enhanced tumor incidence, growth of the primary tumor, and tumor metastases. These data highlight the diverse roles that heparanase plays in different cell types, tissues, and immune cell activation states.

Heparanase has an emerging role in major human diseases, such as cancer, inflammatory diseases, thrombosis, atherosclero-

sis, and various rare diseases (10, 46–48). We have explored the importance of heparanase production by NK cells in their infiltration into Matrigel and tumors, but it might be interesting to assess the impact of heparanase loss in other NK cell–dependent conditions such as Herpes virus infections or recruitment into inflammatory sites caused by TLR agonists or similar danger signals, in which NK cells are known to be critical in host defense (49, 50). However, heparanase is best known for its involvement in tumor growth and angiogenesis, metastasis, and chemoresistance (10, 46), indicating that heparanase is a promising therapeutic target for cancer therapy. Preclinical studies in mice clearly showed that inhibition of heparanase reduces the growth and metastasis of solid tumors (51) and hematological malignancies (52, 53). The first clinical trials targeting heparanase by HS mimetics (PI-88, PG545, roneparstat, and necuparanib) in patients look partially promising (46). However, the increased tumor susceptibility of *Hpse*$^{fl/fl}$ *NKp46-iCre* mice indicates that the cell-intrinsic production of heparanase in NK cells is important for their potential to invade and suppress tumors. It is also notable that we found that potent immunotherapies such as high-dose IL-2 and the anti–PD-1/anti-CTLA4 combination were poorly effective when NK cells lacked heparanase. In addition to potential consequences for combination therapies, these findings suggest that innate or adaptive resistance mechanisms used by tumors could potentially include various methods to reduce NK cell heparanase expression or activity. Our data suggest that inhibiting heparanase in tumor patients may not only affect tumor growth and metastasis but may also have adverse effects on the ability of NK cells to be recruited to the appropriate position to exert their function. Our data advocate a more selective targeting of heparanase in tumor cells that would avoid the potentially adverse effect of reducing effector T cell or NK cell infiltration into tumors. In line with this theory, the translation of heparanase function has been exploited in humans by engineering CAR T cells overexpressing heparanase (21). Such T cells showed improved ECM degradation in vitro and efficiently infiltrated solid tumors in vivo, ultimately leading to improved antitumor activity. Our study strongly suggests that similarly maintaining and/or enhancing heparanase expression in NK cells will improve NK cell–based anticancer immunotherapy.

Methods

Enrichment of human cells from PBMCs

PBMCs were isolated from buffy coats and blood using Ficoll-Paque Premium (GE Healthcare). For the generation of iDCs, PBMCs were resuspended in HBSS (Invitrogen, Thermo Fisher Scientific) containing 5% heat-inactivated fetal calf serum (HIFCS) and incubated for 30 to 45 minutes. Adherent monocytes were cultured in mixed leukocyte culture–conditioned (MLC-conditioned) media (consisting of DMEM supplemented with 4 mg/ml D-glucose, 6 μg/ml folic acid, 3.6 μg/ml ʟ-asparagine, 116 μg/ml ʟ-arginine, 3.7 mg/ml NaHCO₃, 10% FCS, 2 mM ʟ-glutamine, 1 mM HEPES, 1 mM sodium pyruvate, 0.1 mM 2-mercaptoethanol, 100 U/ml penicillin, 50 μg/ml streptomycin, and 100 μg/ml neomycin) supplemented with 50 ng/ml granulocyte macrophage–CSF (GM-CSF) and 20 ng/ml IL-4. On day 4, nonadherent monocyte-derived i-DCs were purified by FACS sorting of CD3⁻CD14⁻ CD56⁻CD19⁻CD209⁺ cells on a BD FACS Vantage SE Diva Option

Sorter (BD Biosciences). NK cells were isolated by negative depletion using the RosetteSep Human NK cell Enrichment Cocktail (STEM-CELL Technologies; catalog 15025) as described previously (54). The purity of NK cells was assessed by flow cytometry after staining with the BD Simultest CD3/CD16⁺CD56 Kit (BD Biosciences).

Human NK cell activation and culture

The B lymphoblastoid cell line (B-LCL) used to activate NK cells in culture has been described elsewhere (55). B-LCL and NK cells were resuspended in MLC media supplemented with 80 U/ml recombinant human IL-2 and cocultured at a ratio of 10⁵:10⁴, respectively. After 18 days of cocultivation, NK cells were further stimulated for 20 hours with 2 ng/ml PMA and 0.1 μM ionomycin in order to generate a-NK cells.

Mice

C57BL/6J WT mice were purchased from the Walter and Eliza Hall Institute for Medical Research or bred in-house at the QIMR Berghofer Medical Research Institute and the La Trobe Animal Research and Teaching Facility. *Hpse*$^{-/-}$ (6), *Hpse*$^{fl/fl}$ (6), *NKp46-iCre* knock-in (56) and immunodeficient *Rag2*$^{-/-}$ *Il2rg*$^{-/-}$ (57, 58) mice were on a C57BL/6 background and bred at the La Trobe Institute for Molecular Science and the QIMR Berghofer Medical Research Institute and were used between the ages of 6 and 16 weeks. Studies involving *Hpse*$^{fl/fl}$ *NKp46-iCre* mice were conducted in a blinded manner. Animals were randomly assigned to groups.

Experimental tumor models

B16F10 (ATCC), RM-1 (provided by Pamela Russell, University of Sydney, Sydney, Australia), and E0771 (provided by Robin Anderson, Peter MacCallum Cancer Centre, Melbourne, Australia) cell lines have all been previously described (26, 59). The cell lines were maintained in complete DMEM (cDMEM) containing 10% FBS, 100 U/ml penicillin, 100 μg/ml streptomycin, and 2 mM glutamax (Gibco, Thermo Fisher Scientific). LWT1 (60) and RMA-S-RAE-1β (25) cell lines were cultured in complete RPMI 1640 (cRPMI) media containing 10% FBS, 100 U/ml penicillin, 100 μg/ml streptomycin, 2 mM glutamax, 55 μM 2-mercaptoethanol, HEPES, and sodium pyruvate. For primary tumor growth, 5×10^6 RMA-S-RAE-1β cells in a volume of 100 μl plain media were transplanted s.c. onto the right hind flank of male mice. The tumor growth was measured every 2 to 3 days with a caliper square as the product of 2 perpendicular diameters (mm²). For the MCA-induced fibrosarcoma model, male mice were injected s.c. into the right hind flank with 100 μg methylcholanthrene (Sigma- Aldrich) in 0.1 ml corn oil. Mice were monitored weekly for the development of fibrosarcoma. Tumors greater than 3 mm in diameter with progressive growth were counted as positive. For experimental metastasis, 1 × 10⁵ RM-1 prostate cancer cells, 1 × 10⁵ to 5 × 10⁵ B16F10 melanoma cells, or 7.5 × 10⁵ LWT1 (*BRAF*^{V600E}-mutant) melanoma cells were injected i.v. in a volume of 200 μl plain media. Some groups of mice were injected i.p. with PBS or 100,000 IU IL-2 on days 0, 1, 2, 3, and 4 after tumor inoculation; some groups of mice received i.p. injections of cIg (hamster Ig) or anti–PD-1 (RMP1-14, rat IgG2a) plus anti-CTLA4 (UC10-4F10, hamster IgG, provided by Jeffrey Bluestone [UCSF, San Francisco, California, USA]) on days 0 and 3 after tumor inoculation. NK cells present in the lung were quantified by flow cytometry 24 hours after the i.v. injection of 5 × 10⁵ B16F10 cells. For spontaneous lung metastases, 2 × 10⁴ E0771 mammary carcinoma cells were

injected orthotopically into the mammary gland in 50 µl plain media. Some mice were treated with 50 µg cIg (rabbit Ig) or anti–asialo-GM1 on days –1, 0, 7, 14, and 23 after tumor transplantation. The tumors were removed surgically on day 12. Lung metastases were quantified on day 12 after the injection of RM-1, on day 14 after the injection of B16F10 and LWT1, or on day 35 after the injection of E0771 by counting the number of macrometastases under a dissecting microscope.

Organ preparation and purification of mouse conventional NK and ILC1 cells

Mouse livers and lungs were perfused with cold PBS postmortem before harvesting the organs. Livers were prepared as described elsewhere (61). Lungs were cut into fine pieces and incubated in 1 mg/ml collagenase type 4 (Worthington Biochem) and 20 µg/ml DNAse I (Roche) in plain DMEM for 45 minutes at 37°C. Single-cell suspensions from all organs (blood, liver, lung, spleen, and bone marrow) were treated with ammonium chloride potassium (ACK) buffer (0.15 M NH_4Cl, 1 mM $KHCO_3$, and 0.1 mM Na_2 EDTA) to deplete erythrocytes. For NK cell sorting, splenocytes or bone marrow single-cell suspensions from 2 to 6 mice were pooled and enriched for NK cells using the NK Cell Isolation Kit II (Miltenyi Biotec). Following magnetic separation on an autoMACS Separator (Miltenyi Biotec), conventional NK cells were gated as $TCR\beta^-NK1.1^+NKp46^+DX5^+$ cells and sorted on a FACSAria II (4 lasers; BD Biosciences). ILC1 cells were FACS sorted from liver lymphocytes and gated as $CD45^+TCR\beta^-NK1.1^+NKp46^+DX5^-CD49a^+$ cells.

Mouse NK cell activation

In vitro. Sorted mouse NK cells were plated at a density of 1×10^5 to 5×10^5 cells/96-well plate/200 µl in cRPMI. Cytokine concentrations included 300–600 U/ml recombinant human IL-2 (provided by Chiron Corporation), 3–100 ng/ml recombinant IL-15/IL-15R complex (eBioscience, referred to herein as IL-15), 1 ng/ml recombinant IL-12 (eBioscience), and 10 ng/ml recombinant IL-18 (R&D Systems). For NK receptor cross-linking, wells were coated with 2 µg anti-NK1.1 (PK136) or 8 µg anti-Ly49D per 96-well plate and incubated overnight at 4°C.

In vivo. Mice were injected i.p. with 250 µg poly(I:C) acid sodium salt (Sigma-Aldrich) dissolved in 200 to 250 µl PBS and analyzed after 24 hours. Alternatively, mice were injected i.p. with 0.2 mg/30 g body weight LPS (Sigma-Aldrich). After 6 hours, blood was drawn retroorbitally, and serum cytokine levels (IFN-γ and TNF) were determined with a Flex Set Multiplex Cytometric Bead Array (CBA) (BD Biosciences). Spleens were harvested, and the production of IFN-γ by NK cells was analyzed by flow cytometry.

Heparanase expression

DNA analysis. DNA was purified from FACS-sorted mouse NK cells using QuickExtract DNA Extraction Solution (Epicentre). The primer sets and conditions for expression of the mouse *Hpse* gene have been published previously (6). For genotyping of the *NKp46-iCre* allele, the following primers were used in 1 reaction (giving rise to a product of approximately 400 bp for the WT and 650 bp for the knock-in alleles, respectively): *NKp46-WT*, forward: GAGAAGATGGAGAATG-CAGCA; *NKp46-WT*, reverse: AGTTCAATTCCCGGCAACAT; and *NKp46-iCre*, forward: TGTCTGGTGTGGCTGATGAC.

mRNA analysis. At least 5×10^6 enriched human NK cells were pelleted and lysed in TRIzol (Invitrogen, Thermo Fisher Scientific) or Ribo-Zol RNA Extraction Reagent (Amresco) and processed according to the

manufacturer's instructions. The dried RNA pellet was reconstituted in 50 µl RNA Storage Solution (Ambion, Applied Biosystems). cDNA was generated from total RNA using the iScript Select cDNA Synthesis Kit (Bio-Rad). For human *HPSE* amplification, reverse transcription PCR (RT-PCR) was performed using the Power SYBR Green System (Applied Biosystems). Primer sequences amplifying the human cDNA were as follows: *HPSE*, forward: GTTCCTGTCCGTCACCATTGA; *HPSE*, reverse: CTTTGGAGAACCCAGGAGGAT; ubiquitin C (*UBC*), forward: TGAAGAGAATCCACAAGGAATTGA; and *UBC*, reverse: CAA-CAGGACCTGCTGAACACTG. *UBC* and *HPSE* amplicons were used to set up the standard curves to obtain absolute copy numbers. *HPSE* was cloned into the pCDNA3 vector and *UBC* into the pCR3.1 vector. The housekeeping gene *UBC* was used as the baseline control for internal gene expression (62). For mouse *Hpse*, cDNA was amplified using FastStart SYBR Green Master (Roche) using the Agilent Mx3000P qPCR System (Agilent Technologies) and the following primers: *Hpse*, forward: CGTCTATCACCCACGATATC; *Hpse*, reverse: CAGTTGGA-CAGATTTAGGAAG; *Gapdh*, forward: TTCCGTGTTCCTACCCCCA; and *Gapdh*, reverse: GCTTCACCACCTTCTTGATGTC.

FACS analysis. Human NK cells (2×10^4 to 4×10^4) were stained for cell-surface antigens before using the Cytofix/Cytoperm Fixation/Permeabilization Solution Kit (BD Biosciences) for the intracellular staining of human heparanase. Samples were analyzed on BD FACS-can or BD LSR I flow cytometers (BD Biosciences).

Western blot analysis. Purified mouse NK cells were lysed in RIPA buffer (Sigma-Aldrich) supplemented with cOmplete Protease Inhibitor (Roche) for 15 minutes. Equal amounts of protein (1–5 µg) were run on SDS-page gels (4%–15% Precast Mini PROTEAN TGX; Bio-Rad). Proteins were transferred to PVDF membranes using the TurboBlot Transfer System (Bio-Rad). The membrane was blocked for 1 hour in 5% skim milk powder before the addition of one of the following primary antibodies: anti-HPSE (Abcam; catalog ab85543; diluted 1:1,000 or Insight Biotechnology; catalog TA332866; diluted 1:4,000) or anti-β-actin (Cell Signaling Technology; catalog 4967; diluted 1:1,000). After overnight incubation, the HRP-conjugated anti-rabbit antibody (Cell Signaling Technology; catalog 7074; diluted 1:5,000–1:20,000) was applied for 40 minutes. Proteins were visualized by x-ray film detection using ECL Prime Western Blotting Detecting Agent (GE Healthcare Life Sciences).

Heparanase enzymatic activity assay

Functional human HPSE activity was measured as described previously (63, 64) with the following modification: for inhibition studies, 1 IU heparin was diluted in water. Samples were incubated at 37°C for 16 hours. A pony vial was filled with Ready Safe Scintillation Fluid (Beckman Coulter), distilled H_2O, and 20 µl sample mixture (5 pMol ^3H–heparan sulphate [provided by C. Freeman [Australian National University, Canberra, Australia]], 2 µg BSA, 10 mM *N*-acetyl mannosamine, 80 mM sodium acetate buffer, pH 5.1, and 0.15 % Triton X-100. Samples were counted in a Tri-Carb 1900CA or Tri-Carb 1500 scintillation machine (Packard) for 1 to 5 minutes.

For mouse HPSE, heparanase enzymatic activity was determined using a time-resolved fluorescence energy transfer–based (TR-FRET–based) assay (Cisbio). Briefly, NK cells were enriched from splenocytes using an EasySep NK Enrichment Kit (STEMCELL Technologies) and lysed in 1% CHAPS/DMG. Equal concentrations of lysates were diluted 1:1 in buffer (20 mM Tris-HCl, 0.15 M NaCl, and 0.1% CHAPS, pH 5.5) before the addition of biotin-HS-Eu(K) [0.7 µg/ml biotin-HS-

Eu(K) and 0.2 M NaCH$_3$CO$_2$, pH 5.5], and the reaction was incubated at 37°C. After 2 hours, 1 μg/ml strepavidin-XL665 (in 0.1 M sodium phosphate, pH 7.5, 1.2 M KF, 0.1% BSA, and 2 mg/ml heparin) was added, and the reaction was incubated in the dark for 16 hours at room temperature. After excitation at 315 nm, the emission was measured at both 620 nm and 668 nm. The percentage of HS degradation was calculated in relation to FRET-positive or -negative samples (i.e., the presence or absence of XL665-conjugated streptavidin, respectively, in the absence of heparanase). To determine the activity per microgram of protein, the final percentage of HS degradation was divided by the absolute mass of the lysates assayed.

Enzymatic degradation of the ECM
^{35}S-labeled ECM (^{35}S-ECM) plates were prepared as described by Vlodavsky (65) with the following modification: 6-well plates were precoated with 2 ml of 0.2% (w/v) gelatine/PBS for 16 hours at 4°C. PF-HR9 cells were seeded at 5 × 10^7 cells per well in PF-HR9 ECM media (10% FCS/high-glucose DMEM supplemented with 50 μg/ml ascorbic acid, 100 U/ml penicillin, 50 μg/ml streptomycin, 100 μg/ml neomycin and 4% [w/v] dextran T40) in a pretreated 6-well plate, together with 40 μCi ^{35}S (Na$_2$SO$_4$; PerkinElmer). On day 2, cultures were fed with 0.5 ml PF-HR9 ECM media. On day 4, cultures were fed with 0.5 ml PF-HR9 media and 20–40 μCi ^{35}S. On day 6, cells were lysed by discarding culture supernatant and incubating with warm NH$_4$OH lysis solution (PBS, 20 mM NH$_4$OH, and 0.5% Triton X-100) at 37°C for 5 to 10 minutes. Cells (2 × 10^6) per ^{35}S-ECM plate were seeded in culture media (0.074 g/l NaHCO$_3$/MLC, 10% FCS, 0.1 M L-glutamine, 0.1 M sodium pyruvate, 0.1 M 2-mercaptoethanol, 100 U/ml penicillin, 50 μg/ml streptomycin, 100 μg/ml neomycin, and 20,000 U/ml recombinant human IL-2, pH 6.0) and incubated for 16 to 22 hours at 37°C. Culture supernatant was harvested and centrifuged at 320 RCF for 10 minutes before supernatant was passed through Amicon Centriprep Ultracel YM-10 or Ultra Ultracel 10k Filter Units (EMD Millipore) at 2,150 RCF. Supernatant (400 μl) was added to 3.6 ml Ready Safe Scintillation Fluid (Beckman Coulter). Samples were counted on a Tri-Carb 1900CA or Tri-Carb 1500 scintillation machine (Packard) for 5 minutes.

Flow cytometry
Single-cell suspensions were prepared as described above and incubated in 2.4G2 (anti-CD16/32) to block nonspecific Fc receptor binding. Cells were washed with FACS buffer (1% FBS and 2 mM EDTA in PBS) and incubated for 20 minutes with diluted antibodies. The following reagents and anti-mouse antibodies (clones) were purchased from Bio-Legend: 7-AAD; anti-CD4 (clone RM4-5); anti-CD8 (clone 53-6.7); anti-CD11b (clone M1/70); anti-CD107a (clone 1DB4); anti-CD226 (clone 480.1); anti–IFN-γ (clone XMG1.2); anti-NKp46 (clone 29A1.4); anti-CD62L (clone Mel-14); anti-CXCR4 (clone L276F12); anti-TCRβ (clone H57-597); and a Zombie Yellow Fixable Viability Kit; from BD Biosciences: annexin V; anti-CD122 (clone TM-β1); anti-NK1.1 (clone PK136); and anti–Ki-67 (clone B56); from Sigma-Aldrich: propidium iodide; from R&D Systems: anti-CCR2 (clone 475301); from eBioscience: anti-CD27 (clone LG.7F9); anti-CD49b (clone DX5); anti-CXCR3 (clone CXCR3-173); anti-KLRG1 (clone 2F1); and anti-NKG2A/C/E (clone 20d5); and from Miltenyi Biotec: anti-CD45.2 (clone 104-2); anti-CD49a (clone REA493); and anti-NKG2D (clone CX5). The following anti-human antibodies were purchased from R&D Systems: anti-CD209 (catalog FAB161P); BD Biosciences: anti-CD3 (catalog 555332); anti-CD14 (cat-

alog 347493); and anti-CD56 (catalog 340410); BioLegend: anti-CD19 (catalog 302206); Insight Biopharmaceuticals: anti-heparanase (catalog INS-26-1-0000-21); and Chemicon: sheep anti-mouse IgG-PE F(ab′)2 (AQ326F). Apoptosis was determined by staining with annexin V and propidium iodide in Annexin V Binding Buffer (BD Biosciences). Degranulation was measured by CD107a staining for 4 hours in the presence of GolgiPlug and GolgiStop (BD Biosciences). Intracellular IFN-γ staining was performed using BD Fixation and Permeabilization Solution. Cytokine release into cell culture supernatants was determined with a CBA Flex Set Multiplex (BD Biosciences). To obtain absolute counts, equal amounts of Liquid Counting Beads (BD Biosciences) were added to the samples shortly before analysis. Single-cell suspensions were analyzed on a BD FACScan, a BD LSR I, or a BD FACS Fortessa Flow Cytometer (4 or 5 lasers), and the analysis was performed using FlowJo software, version 10 (Tree Star).

Proliferation assays
To assess in vitro proliferation, purified NK cells were labeled with 1 μM CTV (Thermo Fisher Scientific) and incubated at 37°C for 72 hours with different concentrations of IL-15 before flow cytometric analysis. To measure in vivo proliferation, FACS-sorted NK cells were labeled with 0.5 μM CFSE (BioLegend) and injected i.v. into recipient *Rag2*$^{-/-}$ *Il2rg*$^{-/-}$ mice (2 × 10^5 cells/200 μl/mouse). The indicated organs were processed for flow cytometric analysis 3 days after transplantation.

Migration and invasion assays
To measure in vitro migration, FACS-purified splenic NK cells were activated overnight in 100 ng/ml IL-15, 1 ng/ml IL-12, and 10 ng/ml IL-18 before being resuspended in plain RPMI containing 1% FBS and loaded onto Corning Transwell inserts (7.5 × 10^4 cells per 24-well plate, 8-μm pores). NK cells were allowed to migrate toward chemo-attractant-containing media (20 ng/ml CXCL10 [R&D Systems] in cRPMI). The number of migrated cells was determined after 17 hours by manual cell counting using a Neubauer chamber. In vivo invasion of lymphocytes into Matrigel plugs was determined 72 hours after the s.c. injection of 100 μl ice-cold growth factor–reduced Matrigel diluted to a concentration of 5 mg/ml in PBS (Corning Matrigel Growth Factor Reduced Basement Membrane Matrix). The plugs were digested by 1 mg/ml collagenase type 4 (Worthington Biochem) and 20 μg/ml DNAse I (Roche) in plain DMEM, with slight agitation for 45 minutes at 37°C, followed by flow cytometric analysis.

Cytotoxicity assays
NK cell cytotoxicity against YAC-1 and B16F10 target cells was tested using freshly isolated splenocytes or splenic NK cells stimulated with IL-2 (1,000 U/ml) for 5 days. Target cells were labeled with 1 μM CTV to distinguish them from effector cells and coincubated with effector cells for 4 hours at different E/T ratios. Tumor cell lysis was determined by staining for annexin V/7-AAD in Annexin V Binding Buffer (BD Biosciences).

Immunofluorescence and image analysis
RMA-S-RAE-1β tumors were excised on day 5 and fresh frozen in PELCO Cryo-embedding Compound. Frozen sections were cut from the tumors and fixed in 4% paraformaldehyde. Sections were stained with anti-NKp46 (R&D Systems; catalog AF2225), detected by tyramide signal amplification (Cy3; PerkinElmer), and counterstained with DAPI. Tiled images of the whole tumor section were captured on

a Zeiss 780 laser-scanning confocal microscope (Oberkochen) using a ×20 objective (0.8 NA). NKp46+ cells were automatically detected using Imaris (Bitplane). The boundary of the tumor was identified by a minimum of 2 independent reviewers to calculate the tumor area. The distance of NKp46+ cells from the edge of the tumor as a percentage of the total distance from the edge to the center of the tumor was calculated using MATLAB (MathWorks). Frequency distribution statistics were performed on the percentage of distance from the edge to the center of the tumor using a bin width of 10% (GraphPad Software).

Statistics

Statistical analysis was performed using Graphpad Prism, version 7.01 (GraphPad Software). Data were considered statistically significant at a P value of 0.05 or less. Data were compared using a Mann-Whitney U test, Student's t test, 1-way ANOVA with Tukey's post test, 2-way ANOVA, or log-rank Mantel-Cox test.

Study approval

Human peripheral blood was obtained with consent from healthy donors by ACT Pathology at the Canberra Hospital (Garran, Australia). Fresh buffy coats were obtained from the ACT Red Cross Blood Transfusion Service (Canberra, Australia). Ethics approval for the collection and use of human blood was given by the ACT Health Research Ethics Committee and the Australian National University Human Ethics Committee (FHE09/R16). Anonymity of donors was achieved by labeling buffy coat donor samples with numbers corresponding to the serial found on the buffy coat, and individual donors were given a code only known within the laboratory. All mouse experiments were approved by the QIMR Berghofer Medical Research Institute Animal Ethics Committee and the La Trobe Animal Ethics Committee.

Author contributions

EMP, MDH, and MJS designed the research study; EMP, AJM, KK, DSB, KN, LT, KJG, DYY, IKHP, NB, and FSFG conducted experiments and acquired and analyzed the data; EMP, MDH, and MJS wrote the manuscript. All authors contributed to the writing of the manuscript.

Address correspondence to: Mark J. Smyth, Immunology in Cancer and Infection Laboratory, QIMR Berghofer Medical Research Institute, 300 Herston Road, Herston, Queensland 4006, Australia. Phone: 61.7.3845.3957; Email: mark.smyth@qimrberghofer.edu.au. Or to: Mark D. Hulett, Department of Biochemistry and Genetics, La Trobe Institute for Molecular Science, La Trobe University, Science Drive, Bundoora, Victoria 3083, Australia. Phone: 61.3.9479.6567; Email: m.hulett@latrobe.edu.au.

1. Halama N, et al. Natural killer cells are scarce in colorectal carcinoma tissue despite high levels of chemokines and cytokines. *Clin Cancer Res*. 2011;17(4):678–689.
2. Cantoni C, et al. NK cells, tumor cell transition, and tumor progression in solid malignancies: New hints for NK-based immunotherapy? *J Immunol Res*. 2016;2016:4684268.
3. Fridman WH, Pagès F, Sautès-Fridman C, Galon J. The immune contexture in human tumours: impact on clinical outcome. *Nat Rev Cancer*. 2012;12(4):298–306.
4. Sarrazin S, Lamanna WC, Esko JD. Heparan sulfate proteoglycans. *Cold Spring Harb Perspect Biol*. 2011;3(7):a004952.
5. Zcharia E, et al. Newly generated heparanase knock-out mice unravel co-regulation of heparanase and matrix metalloproteinases. *PLoS ONE*. 2009;4(4):e5181.
6. Poon IK, et al. Mice deficient in heparanase exhibit impaired dendritic cell migration and reduced airway inflammation. *Eur J Immunol*. 2014;44(4):1016–1030.
7. Abboud-Jarrous G, et al. Cathepsin L is responsible for processing and activation of prohepara-

nase through multiple cleavages of a linker segment. *J Biol Chem*. 2008;283(26):18167–18176.
8. Cui H, et al. Heparanase expression upregulates platelet adhesion activity and thrombogenicity. *Oncotarget*. 2016;7(26):39486–39496.
9. Fux L, Ilan N, Sanderson RD, Vlodavsky I. Heparanase: busy at the cell surface. *Trends Biochem Sci*. 2009;34(10):511–519.
10. Sanderson RD, Elkin M, Rapraeger AC, Ilan N, Vlodavsky I. Heparanase regulation of cancer, autophagy and inflammation: new mechanisms and targets for therapy. *FEBS J*. 2017;284(1):42–55.
11. Goldshmidt O, et al. Heparanase mediates cell adhesion independent of its enzymatic activity. *FASEB J*. 2003;17(9):1015–1025.
12. Gilat D, et al. Molecular behavior adapts to context: heparanase functions as an extracellular matrix-degrading enzyme or as a T cell adhesion molecule, depending on the local pH. *J Exp Med*. 1995;181(5):1929–1934.
13. Fux L, et al. Structure-function approach identifies a COOH-terminal domain that mediates heparanase signaling. *Cancer Res*. 2009;69(5):1758–1767.
14. Hulett MD, Freeman C, Hamdorf BJ, Baker RT,

Harris MJ, Parish CR. Cloning of mammalian heparanase, an important enzyme in tumor invasion and metastasis. *Nat Med*. 1999;5(7):803–809.
15. Vlodavsky I, et al. Mammalian heparanase: gene cloning, expression and function in tumor progression and metastasis. *Nat Med*. 1999;5(7):793–802.
16. Hammond E, Khurana A, Shridhar V, Dredge K. The role of heparanase and sulfatases in the modification of heparan sulfate proteoglycans within the tumor microenvironment and opportunities for novel cancer therapeutics. *Front Oncol*. 2014;4:195.
17. Ostrovsky O, et al. Modification of heparanase gene expression in response to conditioning and LPS treatment: strong correlation to rs4693608 SNP. *J Leukoc Biol*. 2014;95(4):677–688.
18. Benhamron S, et al. Dissociation between mature phenotype and impaired transmigration in dendritic cells from heparanase-deficient mice. *PLoS ONE*. 2012;7(5):e35602.
19. Morris A, et al. The role of heparanase in pulmonary cell recruitment in response to an allergic but not non-allergic stimulus. *PLoS ONE*. 2015;10(6):e0127032.
20. Stoler-Barak L, et al. Heparanase of murine effec-

tor lymphocytes and neutrophils is not required for their diapedesis into sites of inflammation. *FASEB J*. 2015;29(5):2010–2021.

21. Caruana I, et al. Heparanase promotes tumor infiltration and antitumor activity of CAR-redirected T lymphocytes. *Nat Med*. 2015;21(5):524–529.

22. Benhamron S, et al. Translocation of active heparanase to cell surface regulates degradation of extracellular matrix heparan sulfate upon transmigration of mature monocyte-derived dendritic cells. *J Immunol*. 2006;176(11):6417–6424.

23. Smyth MJ, Crowe NY, Godfrey DI. NK cells and NKT cells collaborate in host protection from methylcholanthrene-induced fibrosarcoma. *Int Immunol*. 2001;13(4):459–463.

24. Diefenbach A, Jensen ER, Jamieson AM, Raulet DH. Rae1 and H60 ligands of the NKG2D receptor stimulate tumour immunity. *Nature*. 2001;413(6852):165–171.

25. Hayakawa Y, et al. Cutting edge: tumor rejection mediated by NKG2D receptor-ligand interaction is dependent upon perforin. *J Immunol*. 2002;169(10):5377–5381.

26. Blake SJ, et al. Suppression of metastases using a new lymphocyte checkpoint target for cancer immunotherapy. *Cancer Discov*. 2016;6(4):446–459.

27. de Andrade LF, Ngiow SF, Martinet L, Smyth MJ. Natural Killer cell control of BRAF(V600E) mutant melanoma during targeted therapy. *Oncoimmunology*. 2015;4(4):e998119.

28. Parish CR, Freeman C, Hulett MD. Heparanase: a key enzyme involved in cell invasion. *Biochim Biophys Acta*. 2001;1471(3):M99–M108.

29. Guillerey C, Huntington ND, Smyth MJ. Targeting natural killer cells in cancer immunotherapy. *Nat Immunol*. 2016;17(9):1025–1036.

30. Levy EM, Roberti MP, Mordoh J. Natural killer cells in human cancer: from biological functions to clinical applications. *J Biomed Biotechnol*. 2011;2011:676198.

31. Wennerberg E, Kremer V, Childs R, Lundqvist A. CXCL10-induced migration of adoptively transferred human natural killer cells toward solid tumors causes regression of tumor growth in vivo. *Cancer Immunol Immunother*. 2015;64(2):225–235.

32. Melero I, Rouzaut A, Motz GT, Coukos G. T-cell and NK-cell infiltration into solid tumors: a key limiting factor for efficacious cancer immunotherapy. *Cancer Discov*. 2014;4(5):522–526.

33. Coca S, et al. The prognostic significance of intratumoral natural killer cells in patients with colorectal carcinoma. *Cancer*. 1997;79(12):2320–2328.

34. Ishigami S, et al. Prognostic value of intratumoral natural killer cells in gastric carcinoma. *Cancer*. 2000;88(3):577–583.

35. Pasero C, et al. Highly effective NK cells are associated with good prognosis in patients with metastatic prostate cancer. *Oncotarget*. 2015;6(16):14360–14373.

36. Qin Z, Kim HJ, Hemme J, Blankenstein T. Inhibition of methylcholanthrene-induced carcinogenesis by an interferon gamma receptor-dependent foreign body reaction. *J Exp Med*. 2002;195(11):1479–1490.

37. Wendel M, Galani IE, Suri-Payer E, Cerwenka A. Natural killer cell accumulation in tumors is dependent on IFN-gamma and CXCR3 ligands. *Cancer Res*. 2008;68(20):8437–8445.

38. Riaz A, Ilan N, Vlodavsky I, Li JP, Johansson S. Characterization of heparanase-induced phosphatidylinositol 3-kinase-AKT activation and its integrin dependence. *J Biol Chem*. 2013;288(17):12366–12375.

39. Gingis-Velitski S, Zetser A, Flugelman MY, Vlodavsky I, Ilan N. Heparanase induces endothelial cell migration via protein kinase B/Akt activation. *J Biol Chem*. 2004;279(22):23536–23541.

40. Parish CR, et al. Unexpected new roles for heparanase in Type 1 diabetes and immune gene regulation. *Matrix Biol*. 2013;32(5):228–233.

41. He YQ, et al. The endoglycosidase heparanase enters the nucleus of T lymphocytes and modulates H3 methylation at actively transcribed genes via the interplay with key chromatin modifying enzymes. *Transcription*. 2012;3(3):130–145.

42. Purushothaman A, Hurst DR, Pisano C, Mizumoto S, Sugahara K, Sanderson RD. Heparanase-mediated loss of nuclear syndecan-1 enhances histone acetyltransferase (HAT) activity to promote expression of genes that drive an aggressive tumor phenotype. *J Biol Chem*. 2011;286(35):30377–30383.

43. Goodall KJ, Poon IK, Phipps S, Hulett MD. Soluble heparan sulfate fragments generated by heparanase trigger the release of pro-inflammatory cytokines through TLR-4. *PLoS ONE*. 2014;9(10):e109596.

44. Gutter-Kapon L, et al. Heparanase is required for activation and function of macrophages. *Proc Natl Acad Sci USA*. 2016;113(48):E7808–E7817.

45. Brennan TV, et al. Heparan sulfate mimetic PG545-mediated antilymphoma effects require TLR9-dependent NK cell activation. *J Clin Invest*. 2016;126(1):207–219.

46. Rivara S, Milazzo FM, Giannini G. Heparanase: a rainbow pharmacological target associated to multiple pathologies including rare diseases. *Future Med Chem*. 2016;8(6):647–680.

47. Goldberg R, et al. Versatile role of heparanase in inflammation. *Matrix Biol*. 2013;32(5):234–240.

48. Vlodavsky I, Blich M, Li JP, Sanderson RD, Ilan N. Involvement of heparanase in atherosclerosis and other vessel wall pathologies. *Matrix Biol*. 2013;32(5):241–251.

49. Lisnić B, Lisnić VJ, Jonjić S. NK cell interplay with cytomegaloviruses. *Curr Opin Virol*. 2015;15:9–18.

50. Della Chiesa M, Marcenaro E, Sivori S, Carlomagno S, Pesce S, Moretta A. Human NK cell response to pathogens. *Semin Immunol*.

2014;26(2):152–160.

51. Dredge K, et al. PG545, a dual heparanase and angiogenesis inhibitor, induces potent anti-tumour and anti-metastatic efficacy in preclinical models. *Br J Cancer*. 2011;104(4):635–642.

52. Weissmann M, et al. Heparanase-neutralizing antibodies attenuate lymphoma tumor growth and metastasis. *Proc Natl Acad Sci U S A*. 2016;113(3):704–709.

53. Ramani VC, et al. Targeting heparanase overcomes chemoresistance and diminishes relapse in myeloma. *Oncotarget*. 2016;7(2):1598–1607.

54. Warren HS, Rana PM. An economical adaptation of the RosetteSep procedure for NK cell enrichment from whole blood, and its use with liquid nitrogen stored peripheral blood mononuclear cells. *J Immunol Methods*. 2003;280(1–2):135–138.

55. Warren HS, Kinnear BF, Witt CS, Christiansen FT. Proliferation of alloreactive human natural killer cells independent of specific allogeneic stimulation. *Int Immunol*. 1994;6(4):507–513.

56. Narni-Mancinelli E, et al. Fate mapping analysis of lymphoid cells expressing the NKp46 cell surface receptor. *Proc Natl Acad Sci U S A*. 2011;108(45):18324–18329.

57. DiSanto JP, Müller W, Guy-Grand D, Fischer A, Rajewsky K. Lymphoid development in mice with a targeted deletion of the interleukin 2 receptor gamma chain. *Proc Natl Acad Sci U S A*. 1995;92(2):377–381.

58. Shinkai Y, et al. RAG-2-deficient mice lack mature lymphocytes owing to inability to initiate V(D)J rearrangement. *Cell*. 1992;68(5):855–867.

59. Liu J, et al. Improved efficacy of neoadjuvant compared to adjuvant immunotherapy to eradicate metastatic disease. *Cancer Discov*. 2016;6(12):1382–1399.

60. Ferrari de Andrade L, et al. Natural killer cells are essential for the ability of BRAF inhibitors to control BRAFV600E-mutant metastatic melanoma. *Cancer Res*. 2014;74(24):7298–7308.

61. Hayakawa Y, Andrews DM, Smyth MJ. Subset analysis of human and mouse mature NK cells. *Methods Mol Biol*. 2010;612:27–38.

62. de Mestre AM, Khachigian LM, Santiago FS, Staykova MA, Hulett MD. Regulation of inducible heparanase gene transcription in activated T cells by early growth response 1. *J Biol Chem*. 2003;278(50):50377–50385.

63. Poon IK, et al. Histidine-rich glycoprotein binds heparanase and regulates its enzymatic activity and cell surface interactions. *Int J Biochem Cell Biol*. 2010;42(9):1507–1516.

64. Freeman C, Parish CR. A rapid quantitative assay for the detection of mammalian heparanase activity. *Biochem J*. 1997;325 (Pt 1):229–237.

65. Vlodavsky I. Preparation of extracellular matrices produced by cultured corneal endothelial and PF-HR9 endodermal cells. *Curr Protoc Cell Biol*. 2001;Chapter 10:Unit 10.4.